

Superconductivity of Ultra-fine Tungsten Nanowires Grown by Focused-ion-beam Direct-writing

Wuxia Li,^{1,2,*} J.C. Fenton¹, Changzhi Gu², and P. A. Warburton¹

¹London Centre for Nanotechnology, University College London, 17-19 Gordon Street, London, WC1H 0AH, United Kingdom

²Institute of Physics, Chinese Academy of Sciences, Beijing 100190, China

Abstract

The electrical properties of lateral ultrafine tungsten nanowires, which were grown by focused-ion-beam-induced deposition with 1 pA ion beam current, were investigated. Temperature-dependent electrical measurements show that the wires are conducting and have a superconducting transition with a transition temperature (T_c) about 5.1 K. Resistance vs temperature measurements reveal that, with decreasing cross-sectional area, the wires display an increasingly broad superconducting transition. A residual resistive tail extending down to the low-temperature region is found only for the thinnest tungsten nanowire, which is 10 nm thick and 19 nm wide. The logarithm of the residual resistance of this wire appears as two linear sections as a function of temperature, one within 300 mK below T_c and the other extending down to the lowest measuring temperature of 4.26 K. Such features have previously been identified with phase slip processes. Our results are suggestive that the focused-ion-beam technique might be a potential approach to fabricate ultra-thin and ultra-narrow nanowires for the study of superconducting suppression in nanoscale materials and for maskless superconducting device fabrication.

PACS: 74.78.Na; 74.81.Bd; 74.62.Yb

Keywords: superconductivity, nanowire, focused-ion-beam, direct-writing

I. Introduction

The superconductivity of a film or nanowire exhibits quasi-two-dimensional or quasi-one-dimensional behaviors when the thickness of the superconducting film or the diameter of the superconducting nanowire is reduced to smaller than the Ginsburg-Landau phase coherence length (ξ) and the magnetic penetration depth (λ).¹⁻⁴ Below the superconducting transition temperature, the resistance of a 1D wire is no longer zero. The nonzero dissipation may be due to thermally activated phase slip (TAPS) or quantum phase slip (QPS) processes.⁵⁻⁶ During a phase slip, the superconducting order parameter fluctuates to zero at some point along the wire; the relative phase across the point slips by 2π , resulting in a voltage pulse and the sum of many such pulses gives a resistive voltage.⁷ A quick approach to probe such phenomena is to examine the temperature-dependent resistance (R-T) and transport (I-V) properties below and near T_c .⁸⁻⁹

The direct fabrication of nano-structures or the modification of existing structures using focused ion beams (FIB) has attracted remarkable interest in recent years. Such a technique offers the means to rapidly develop nanoscale devices in a single processing step in-situ without the demand of time-consuming mask fabrication or extensive prior sample

* Corresponding Author; E-mail: liwuxia@aphy.iphy.ac.cn; tel: +86-10-82649098; fax: +86-10-82648198

preparation. Most importantly, the growth is site specific and using ion beam current as low as 1 pA or lower, true nanoscale wires can be grown; what's more, by simply changing the growth parameters, the composition, thickness and geometry of the deposits can be tuned.⁹⁻¹⁰

Tungsten is one of the most commonly used materials in FIB-CVD. Bulk tungsten has a resistivity of 5 $\mu\Omega$ cm; however, materials grown by the FIB-CVD process contain various impurities including carbon and oxygen from the precursor gas and gallium from the incident ion beam. As a consequence, such deposits have a resistivity of around 200 $\mu\Omega$ cm. Fortunately, compared with the bulk counterpart, despite the increase in the room temperature resistivity, it has been proved to have a significantly enhanced superconducting transition temperature T_c above 5 K, a value technologically-useful above 4.2 K. This opens up the possibility of fabricating novel superconducting devices without mask and other conventional microfabrication techniques.

Thus we have grown ultra-narrow and ultra-thin tungsten nanowires by FIB-CVD using a 1pA ion-beam current. Continuous lateral nanowires 19 nm wide and 10 nm thick were achieved. The thickness and width of wires were controlled by setting different exposure times. The temperature dependent electrical properties were examined by 4-probe measurement after direct writing of the four-terminal configuration in a single FIB run. All the wires are conducting have a superconducting T_c above 5.0 K and can be repeatedly thermally cycled. The transition width was found to be strongly dependent on wire cross-sectional area. The logarithm plot of the residual resistance of the narrowest wire shows two linear sections as a function of temperature, indicating possible phase slip processes. Our results suggest that the focused-ion-beam technique might be a potential approach to fabricate ultra-thin and ultra-narrow wires for the study of superconducting suppression in nanoscale materials, or for maskless superconducting device fabrication.

II. Experimental details

A commercially available FIB (Carl Zeiss XB1540) system utilizing a beam of 30 keV singly-charged Ga^+ ions was used. Tungsten hexacarbonyl ($\text{W}(\text{CO})_6$) gas was injected in the vicinity of the focused beam scanned area through a nozzle and was absorbed onto the surface of the sample. As the beam was scanned over the surface of the sample in the desired pattern, the precursor was decomposed into volatile and non-volatile components. The non-volatile component was deposited on the sample surface whilst the volatile product was removed via the instruments vacuum system. The base pressure before introducing the precursor gas was 2.4×10^{-6} mbar. During deposition the system pressure was in the range of $7.4 - 8.3 \times 10^{-6}$ mbar. Gold contact patterns were formed onto Si substrates with a 200-nm-thick oxidized silicon layer by conventional photolithography-based processes before the W deposition.¹¹

Lateral nanowires with various widths and thicknesses were deposited with a 1 pA ion-beam probe with ion beam exposure time of 10, 15, 25, 35, 40 and 50s, respectively. A larger ion beam current, 20 pA in our experiment was then used to deposit strips as connectors to the large Au contact pads to form a four-terminal device configuration for electrical properties measurements. The width and height of nanowires were measured by *in-situ* SEM and by atomic force microscope (AFM). The microstructure was analyzed by transmission electron microscopy (TEM) for wires deposited on holey carbon TEM grids using the identical condition using for transport property measurement. The chemical composition was obtained by energy dispersive X-ray spectroscopy (EDS) attached to the TEM. Current-biased transport measurements were performed with the sample mounted on a "dip-stick" immersed in a liquid-helium storage dewar. Transport measurements were

performed with a home-made current source and voltage amplifier. All the data acquisition and analysis were controlled by a LabView-based platform.¹⁰

III. Results and discussion

Figure 1 (a) shows a typical SEM top view image of nanowires deposited using a 1 pA ion beam current with various ion beam exposure times. Specifically the widths were 11, 19, 32, 44, 52 and 61 nm for wires deposited with ion beam exposure time of 10, 15, 25, 35, 40 and 50 s, respectively. The wire peak height and width versus the ion beam exposure time is shown in Fig. 1 (b). Nanowires deposited with exposure time less than 10 s were not continuous. For accurate fine-line deposition, it is necessary to use small beam spot size, since larger beam spot size corresponds to larger ion beam current, which leads to an irregular periphery of the deposited area; it also causes line width broadening. To deposit fine and continuous nanowires with size at the resolution limit for the facility, experiments to adjust the beam dwell time, beam spot overlap and other growth parameters are currently underway.

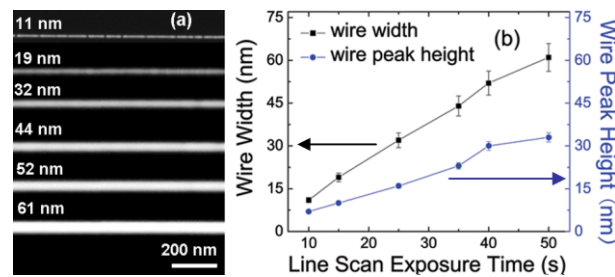


Fig. 1. (a) SEM top view image of lateral tungsten nanowires grown with a 1 pA ion beam current, using exposure time of 10, 15, 25, 35, 40 and 50s respectively; (b) wire width and peak height (measured by atomic force microscope) as a function of the exposure time.

Temperature-dependent resistivity measurements were performed for nanowires with width of 19, 32, 44, 52 and 61 nm and corresponding thickness of 10, 16, 23, 30, 33 nm, respectively. Thinner and narrower lateral wire can be made though at this stage SEM reveals that it is not continuous and, likewise, electrical measurement shows a very large resistance beyond the electronic meter range in this work. The 19 nm wide and 10 nm thick wire is conducting with a room temperature resistivity of 330 $\mu\Omega$ cm. Figure 2 shows a typical four-terminal configuration formed on the 19 nm wide and 10 nm thick nanowire.

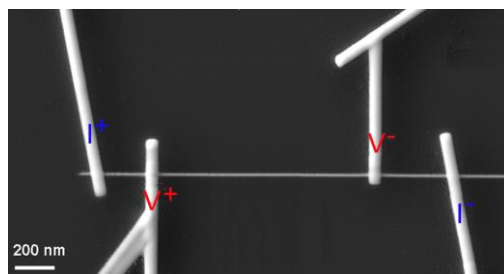


Fig. 2 SEM top view image of a typical four terminal configuration of a lateral tungsten nanowires that is 19 nm wide and 10 nm thick for electrical property measurement.

A constant current of 1.0 μ A was applied to the two outer terminals and the voltage was measured between the other two terminals. All the nanowires show superconducting

transitions above 5.0 K; here T_c is defined as the temperature at which the resistivity falls to 50% of its value at the onset of the transition.

The temperature-dependent normalized resistivity for the 19, 32 and 61 nm wide nanowires is shown in Fig. 3 (a). It can be seen that the transition width of the 19 nm wide sample is much wider than that of the 61 nm wide one. The error bars in Fig. 3(b) correspond to the width of the superconducting transition. It is worth noting that with decreasing cross-sectional area, the wires display increasingly a broad resistive transition. For wire with width larger than 60 nm, the transition width maintains an approximately constant value. We have performed TEM measurements, which confirm that the nanowires do not display any long-range order – rather there are nanocrystallites with grain size on the order of 1 nm. We have also done both electron-energy loss and energy dispersive x-ray spectroscopy on our nanowires, which show that the composition is 48 at% tungsten, 30 at% carbon, 16 at% gallium and 6 at% oxygen. Thus FIB-deposited tungsten nanowires are different from bulk crystalline tungsten in terms of compositional and structural properties besides the dimensionality.

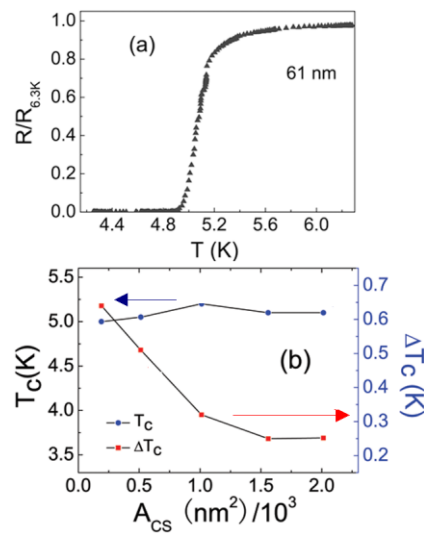


Fig. 3. (a) The temperature dependent normalized resistance of the tungsten nanowires that is 61 nm wide; (b) superconducting transition temperature (T_c) and transition width (ΔT_c) as a function of the cross-sectional area (A_{CS}) of the nanowires.

A residual resistive tail extending down to the low-temperature region is found for wires with width of 19 nm. When the logarithm of the residual resistances is plotted vs temperature, there appear two distinct linear sections (as shown in Fig.4), one within 300 mK below T_c and the other extending down to the lowest measuring temperature of 4.26 K. This is in contrast to the resistance for wires with width larger than 61 nm, which drops precipitously to a constant small value at T_c near 5.1 K. A similar broadening of the transition has been reported on Sn^{12} and GeMo^{13} nanowires and was interpreted as being a consequence of a TAPS process near T_c and QPS in the lower temperature region.^{7,12} However, we have not ruled out the possibility that the resistive tail is somehow associated with inhomogeneities present in the wires on a length scale of around 10 nm.

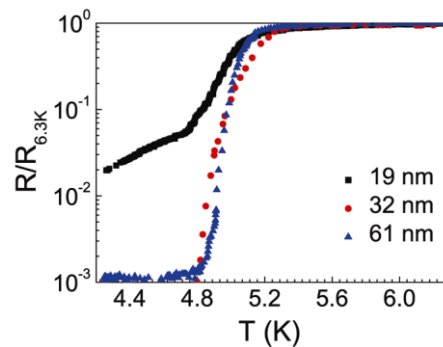


Fig. 4. Normalized resistance vs temperature of the 19, 32 and 61 nm wide nanowires with normalized resistance in the log plot, showing distinct transition characteristics.

To further understand these interesting electrical properties in FIB-deposited nanowires, lower temperature I-V measurements are necessary and would be very helpful. It is reported that the I-V characteristic of a one-dimensional nanowire shows distinct linear branches when the current is reduced with phase-slip centres.¹² Though TAPS and QPS phenomena have been reported on nanoobjects made by techniques such as growth of crystalline Pb and then using FIB milling to cut it into nano bridge structure¹⁴, electrodeposition of Sn nanowires into anodized alumina oxide templates¹², the growth process and device fabrication is complicated. By using FIB-CVD, we are able to direct-write maskless superconducting device structures; we hope our work will inspire further theoretical and experiment effort towards the one-step fabrication of superconducting devices, such as a single photon detector based on the hot-spot formation caused by TAPS.

IV. Conclusion

In summary, using the technique of FIB-CVD, we have grown ultra-thin and ultra-narrow tungsten lateral nanowires with width and thickness comparable to the phase coherence length (ξ) of the bulk material. The electrical transport properties of nanowires with thickness of 10 nm, about 2ξ (for FIB deposited tungsten, ξ is 5.9 nm)¹⁵ and reaching the 1D limit, were found to be distinctly different from those with thickness of 33 nm, in a similar way to results previously interpreted as evidence of phase slip processes¹⁶. Our results suggest that FIB-CVD could be a potential approach to grow nanoscale materials for the observation of superconducting quantum phenomenon and to fabricate maskless superconducting devices in a single writing step.

Acknowledgments

The authors acknowledge Kevin Lee for technical assistance. Yiqian Wang, and D.W. McComb for the HRTEM analysis. This work is supported by the IRC in Nanotechnology, by EPSRC contract EP/F035411/1 and National Natural Science Foundation of China under Grant No.20091021

References

- ¹K. Y. Arutyunov, D. S. Golubev, and A. D. Zaikin, *Phys. Rep.* **464**, 1 (2008).
- ²A. Johansson, G. Sambandamurthy, D. Shahar, N. Jacobson, and R. Tenne, *Phys. Rev. Lett.* **95**, 116805(2005).
- ³F. Altomare, A. M. Chang, M. R. Melloch, Y. Hong, and C. W. Tu, *Phys. Rev. Lett.* **97**, 017001 (2006).
- ⁴J. Wang, X. C. Ma, Y. Qi, Y. S. Fu, S. H. Ji, L. Lu, J. F. Jia, and Q. K. Xue, *Appl. Phys. Lett.* **90**, 113109 (2007).

⁵W. A. Little, Phys. Rev. **156**, 396 (1967).

⁶A. Rogachev, A. T. Bollinger, and A. Bezryadin, Phys. Rev. Lett. **94**, 017004 (2005).

⁷A. Rogachev and A. Bezryadin, Appl. Phys. Lett. **83**, 512 (2003).

⁸M. Tian, J. Wang, N. Kumar, T. Han, Y. Kobayashi, Y. Liu, T. E. Mallouk, and M. H. W. Chan, Nano Lett. **6**, 2773 (2006).

⁹W. Li, J. C. Fenton, Y. Wang, D. W. McComb and P. A. Warburton, J. Appl. Phys. **104**, 093913 (2008).

¹⁰W. Li, J. C. Fenton and P. A. Warburton, IEEE Tran. Super. **19**, 2819 (2009).

¹¹M. Tian, J. Wang, J. S. Kurtz, Y. Liu, M. H. W. Chan, T. S. Mayer, T. E. Mallouk, Phys. Rev. B **71**, 104521 (2005).

¹²N. Lau, N. Markovic, M. Bockrath, A. Bezryadin, and M. Tinkham, Phys. Rev. Lett. **87**, 217003 (2001).

¹³N. Giordano, Phys. Rev. B **41**, 6350 (1990).

¹⁴J. Wang, X. Ma, Y. Qi, S. Ji, Y. Fu, L. Lu, A. Jin, C. Z. Gu, X. C. Xie, M. L. Tian, J. F. Jia, and Q. K. Xue, J. Appl. Phys. **106**, 034301 (2009).

¹⁵E. S. Sadki, S. Ooi, and K. Hirata, Appl. Phys. Lett. **85**, 6202 (2004).

¹⁶G.C. Tettamanzi, C.I. Pakes, A. Potenza, S. Rubanov, C.H. Marrows and S. Praver, Nanotechnology **20** (2009) 465302.